IOP Publishing
Journal of Physics D: Applied Physics
J. Phys. D: Appl. Phys. **53** (2020) 135304 (6pp)
https://doi.org/10.1088/1361-6463/ab66d8

Depth profiling of ion-implanted samples by high-energy electron scattering

H Trombini[1,2], M Vos[1], R G Elliman[1] and P L Grande[2]

[1] Electronic Materials Engineering, Research School of Physics, Australian National University, Canberra, Australia
[2] Ion Implantation Laboratory, Institute of Physics, Federal University of Rio Grande do Sul (UFRGS), CEP 91501-970 Porto Alegre, Brazil

E-mail: maarten.vos@anu.edu.au

Received 8 October 2019, revised 11 December 2019
Accepted for publication 2 January 2020
Published 21 January 2020

Abstract

For heavy ions implanted in low-Z targets it is possible to determine the depth and concentration of introduced heavy impurities by studying the energy spectra of electrons scattered from the surface. Here, we demonstrate this for the case of 30 and 300 keV Au implantation in SiO_2. For high-energy incoming electrons the elastic peak splits up in different components as the recoil losses depends on the mass of the scattering atom. Heavy impurities also affect the partial intensities and hence changes in the shape of the energy loss spectra are observed. These effects are reproduced by a simple model that uses sample composition, atomic elastic scattering cross sections and target dielectric function as input.

Keywords: reflection electron energy loss spectroscopy, ion implantation, depth profiling

(Some figures may appear in colour only in the online journal)

1. Introduction

Electron spectroscopy, in particular photoemission, has been a central tool for studying the near-surface composition of materials. The analysis is typically limited to the near-surface (i.e. 5–10 nm) but can be extended to greater depths (≈50 nm) by using higher energy photons, as available at larger synchrotrons. As an alternative way to probe relatively deep into materials, one can use high-energy incoming electrons (5–40 keV) and study the energy distribution of the scattered electrons. In this case the recoil energy can be used to determine the approximate mass of the scattering atom, and thus the near-surface composition of materials. This technique is often referred to electron Rutherford backscattering spectrometry (ERBS) [1] to stress the similarity to ion-beam based RBS technique. Besides the elastic peak, the measurement can also record those electrons that have made electronic excitations. Then the technique is usually referred to as reflection electron energy loss spectroscopy (REELS) [2].

We will show that the REELS spectrum is sensitive to implanted heavy impurities due to the much larger elastic scattering cross section for electrons of high-Z elements. This strongly affects the partial intensities that make up the REELS spectrum, even for relatively low (a few %) impurity concentrations. A simple model is introduced that describes both the elastic peak and REELS part of the spectra. The study described here is closely related to the analysis of the background of buried layers in Hard-x-ray photoemission (e.g. [3,4]) and relevant for the interpretation of Z-contrast measurement based on backscattered electrons in a scanning electron microscope (e.g. [5]).

2. Experimental details

Samples were taken from a Si wafer with a 1000 Å thick SiO_2 thermally grown oxide layer. Two samples were implanted at UFRGS, one with 30 keV Au ions up to a fluence of 7×10^{15} ions cm^{-2} and another with 300 keV Au ions up to a fluence of 1×10^{16} ions cm^{-2}. The fluence was checked with (ion) RBS and agreement with the nominal value was better than 4%. Based on SRIM [6, 7] the mean depth (straggling) of the ions after implantation under these conditions is 207 Å (44 Å) at 30 keV and 928 Å (152 Å) at 300 keV. The TriDyn software [8] predicts somewhat larger values for the range (straggling) of 250 Å (55 Å) at 30 keV and 1150 Å (225 Å) at 300 keV. These differences are due to the rather

large electronic stopping power SRIM uses for heavy ions in light targets at low energies [9].

These and an unimplanted sample were measured at the high-energy electron scattering spectrometer at the Australian National University. Electron beams with a diameter of 0.2 mm and energy between 5 keV (≈1 nA current) and 40 keV (≈8 nA current) were used and spectra were recorded with an overall resolution of 0.5 eV. The analyser float voltage was scanned, changing the kinetic energy of the electrons that were detected, so the energy loss spectrum could be measured over an extended energy range. The beam current was monitored and the scan would progress to the next voltage after a preset amount of charge was accumulated. The scattering angle was 135°, the incoming beam was along the surface normal ($\theta_0 = 0$), and the outgoing beam was thus at $\theta_1 = 45°$.

3. Theory

Fast charged particles interact with both the nuclei and electrons. In the case of large-angle deflection the electron scatters from a single atom and the interaction can be described as if the atom was a free particle. For the justification and limitation of this approximation see e.g. [10, 11]. Due to their large mass-mismatch the interaction of fast electrons with nuclei results in substantial deflections and a small energy transfer that depends on the mass of the deflecting nucleus (due to the recoil effect). For 40 keV electrons scattering through 135° the (mean) recoil losses for Au, Si and O are 0.4 eV, 2.8 eV and 4.9 eV, respectively. These recoil losses can be resolved experimentally [1].

In contrast, interaction of the projectile electron with the target electrons results in only small deflections but significant energy losses. These inelastic processes can be described using the dielectric theory [2, 12]. The probability of an electron with energy E_0 making an electronic excitation with energy ω per unit path length is given by the differential inelastic inverse mean free path $W_b(\omega, E_0)$:

$$W_b(\omega, E_0) = \frac{1}{\pi E_0} \int_{q_-}^{q_+} \frac{dq}{q} \mathrm{Im}\left[\frac{-1}{\epsilon(\omega, q)}\right], \tag{1}$$

where $q_\pm$ are the limits of kinematically allowed momentum transfers:

$$q_\pm = \sqrt{2ME_0} \pm \sqrt{2M(E_0 - \omega)}, \tag{2}$$

in atomic units. Integrating equation (1) over all energy losses gives the probability that any excitation occurs, which corresponds to the inverse inelastic mean free path $1/\lambda$. $W_b(\omega, E_0)$ normalized to unit area is indicated by $w_b(\omega, E_0)$ and is the probability distribution that a certain loss ω occurs in an inelastic event.

The observed spectra consists of contributions of trajectories with 0 (elastic peak), 1, 2... inelastic events. Inelastic events occur along the trajectory randomly, with an average separation given by λ. As the energy losses considered here are small compared to the incoming energy, we assume the energy-dependence of λ can be neglected. Then the probability that along a trajectory of length L, N statistically-independent inelastic events occur is described by the Poisson distribution [2]:

$$\begin{aligned} p_N(L) &= \frac{(L/\lambda)^N}{N!} e^{-L/\lambda} \\ &= \exp\{N \ln\left(\frac{L}{\lambda}\right) - \frac{L}{\lambda} - \ln\Gamma(N+1)\}, \end{aligned} \tag{3}$$

where the latter expression, using the Γ function is more stable for large N values. The energy distribution of trajectories with only a single inelastic loss event is given by $w_b(\omega, E_0)$. The distribution of those electrons that have had two energy loss events is given by the self-convolution of $w_b(\omega, E_0)$. The distribution after N energy loss events is indicated by $V_N(\omega)$ which is obtained by $(N-1)\times$ convolutions of $w_b(\omega, E_0)$ with itself, where $V_0(\omega) = \delta(\omega)$ i.e. the delta function corresponds to the 'elastic peak'.

Assuming only a single large-angle reflection (i.e. a v-shaped trajectory) the total path length is related to the scattering depth z by:

$$L = z/\cos(\theta_0) + z/\cos(\theta_1) = \alpha z \tag{4}$$

with α describing the relation between L and z. The assumption of v-shaped trajectories also underlies the interpretation of almost all ion-beam based RBS measurements. It is expected a suitable approximation for the near surface area of low-Z targets, when the distances considered are much less than the transport mean free path (≈10^5 Å for 40 keV electrons in low-Z targets). The relation between depth z and number of inelastic events, as well as corresponding relevant energy loss distributions, are illustrated in figure 1.

If we make a few additional simplifying assumptions it is quite straightforward to calculate the ERBS/REELS spectrum using the partial intensity analysis [2]. The first one is that all inelastic events can be described by $W_b(\omega, E_0)$ for SiO_2, i.e. that the effect of the Au impurities on the dielectric function can be neglected and the excitation cross section does not change as the electrons slow down slightly while penetrating the SiO_2 film. We also neglect here the effect of the Si substrate i.e. assume that the SiO_2 layer is infinitely thick. Surface plasmons will not be considered here, as they represent as small effect at these large incoming energies.

As there is only one large angle scattering event in a v-shaped trajectory the electron scatters from either Si, or O or Au. We keep track of which atom we scatter from in the calculation. At a given depth z there is a concentration $c_i(z)$ of elements i. Element i has a differential scattering cross section (DCS) σ_i at 135°. These are taken from the ELSEPA program [13]. The contribution to partial intensity N of element i due to atoms at depth z is given by:

$$\frac{dI_N^i}{dz} = c_i(z)\sigma_i p_N(\alpha z). \tag{5}$$

Integrating over all z gives us I_N^i. Note that:

$$\int_0^\infty p_N(L)dL = 1 \tag{6}$$

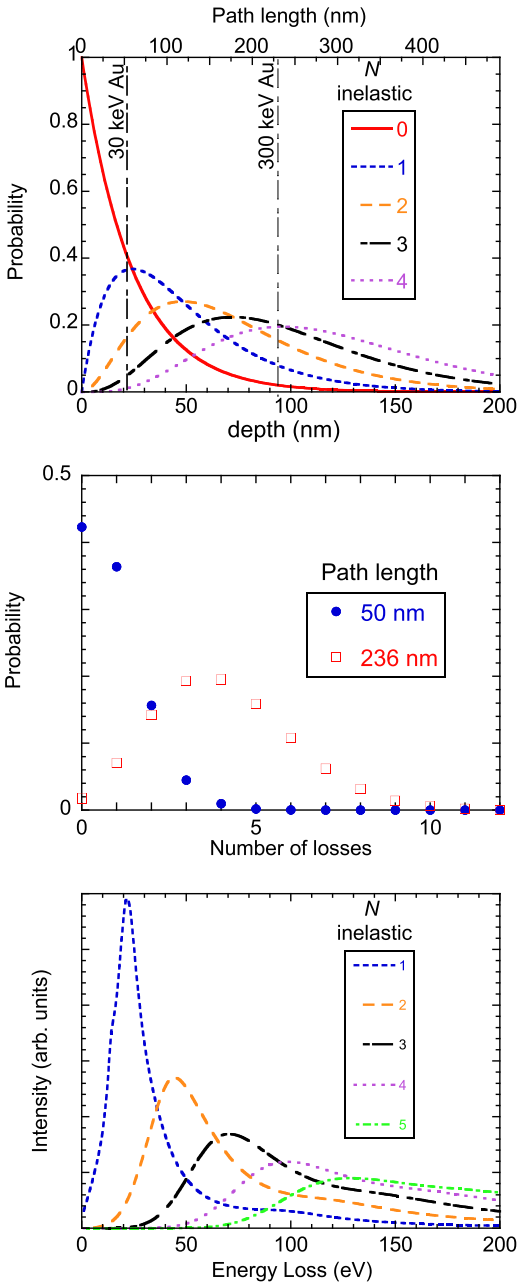

Figure 1. The probability for N inelastic events as a function of the path lenght (top horizontal scale) or depth for the case of 40 keV electrons in SiO_2 (top panel). The approximate mean range of 30 and 300 keV Au ions is indicated as well. The central panel gives the contributions for N inelastic events for a depth corresponding to the mean implantation depth of 30 keV Au (50 nm) and 300 keV Au (235 nm). The lower panel gives the distribution $V_N(\omega)$ i.e. the energy distribution after N inelastic events.

for all N i.e. within the v-shape approximation all partial intensities are the same, if the concentration of element i is homogeneous. Now the energy loss spectrum $S_i(\omega)$ of element i can be calculated as:

$$S_i(\omega) = \sum_N I_N^i V_N(\omega). \tag{7}$$

There is one additional energy loss process we have to incorporate: the recoil losses due to the backscattering event from element i. The recoil losses are centred at the mean recoil energy $E_i^{\mathrm{rec}} = q_{el}^2/2M_i$ with q_{el} the momentum transfer for scattering from atom i (with mass M_i) over 135°. Due to atomic vibrations there is Doppler broadening around this mean value. To take this into account we convolute $S_i(\omega)$ with a Gaussian $G_i(\omega)$, with area 1, centered at E_i^{rec} and a width s_i that reproduces the experimentally observed width of the elastic peak of element i:

$$T_i(\omega) = S_i(\omega) * G_i(\omega). \tag{8}$$

Finally, the experimental spectrum is then obtained by adding the contributions $T_i(\omega)$ of all elements.

4. Experimental results

The electron scattering result for a sample implanted with 7×10^{15} 30 keV Au^+ ions per cm^2 is shown in figure 2 for E_0 values between 5 and 40 keV. The corresponding λ values vary between 108 Å (5 keV) and 600 Å (40 keV). For large incoming energies 3 peaks are seen in the elastic peak, corresponding to Au, Si and O. Measured and simulated spectra (both for the ERBS and the REELS part) were normalised to the Si elastic peak area. With decreasing E_0 the area of the Au peak decreases, as the experiment probes less deep at lower E_0 values.

Surprisingly, the shape of the REELS part of the spectrum, i.e. due to electrons that created also electronic excitations, is also a strong function of E_0. Compared to the spectra from SiO_2 (normalised to equal area of the SiO_2 elastic peak features after implantation) the intensity after Au implantation has increased. For $E_0 = 40$ keV the extra intensity has a maximum near $\omega = 25$ eV and decreases for larger ω values. These larger ω values tend to be associated with longer path lengths and for $E_0 = 40$ keV correspond to depths beyond the Au implantation range. With decreasing E_0 values the extra intensity extends to larger losses and for $E_0 = 5$ keV it increases with ω up to at least 120 eV energy loss. For $E_0 = 5$ keV the λ is such that for low ω values we probe mainly at depth smaller than the Au implantation range.

Simulated spectra were generated based on the theory described above. The number of Au atoms in the sample was taken from the implantation fluence and their depth distribution from the TriDyn simulation. $W_b(\omega, E_0)$ was calculated using the Mermin dielectric function and oscillators essentially as given in [14]. The corresponding λ values were in good agreement with the (relativistic) TPP2M values [15] as obtained via the Quases-IMFP program.

The simulated spectra for the SiO_2 reference sample have a slightly different slope compared to the experiment. This was attributed to the fact that the partial intensities were not constant but increased slowly with N. A good description was obtained by assuming that I_N increases like $1 + 0.03N$. This can be seen as an indication that the trajectories are not all truly v-shaped, or that the dielectric function is slightly different at larger energy loss values [16]. In this way the simulated SiO_2 spectrum was a good description of the measured energy loss spectrum from 0 to 600 eV energy loss. 40 partial

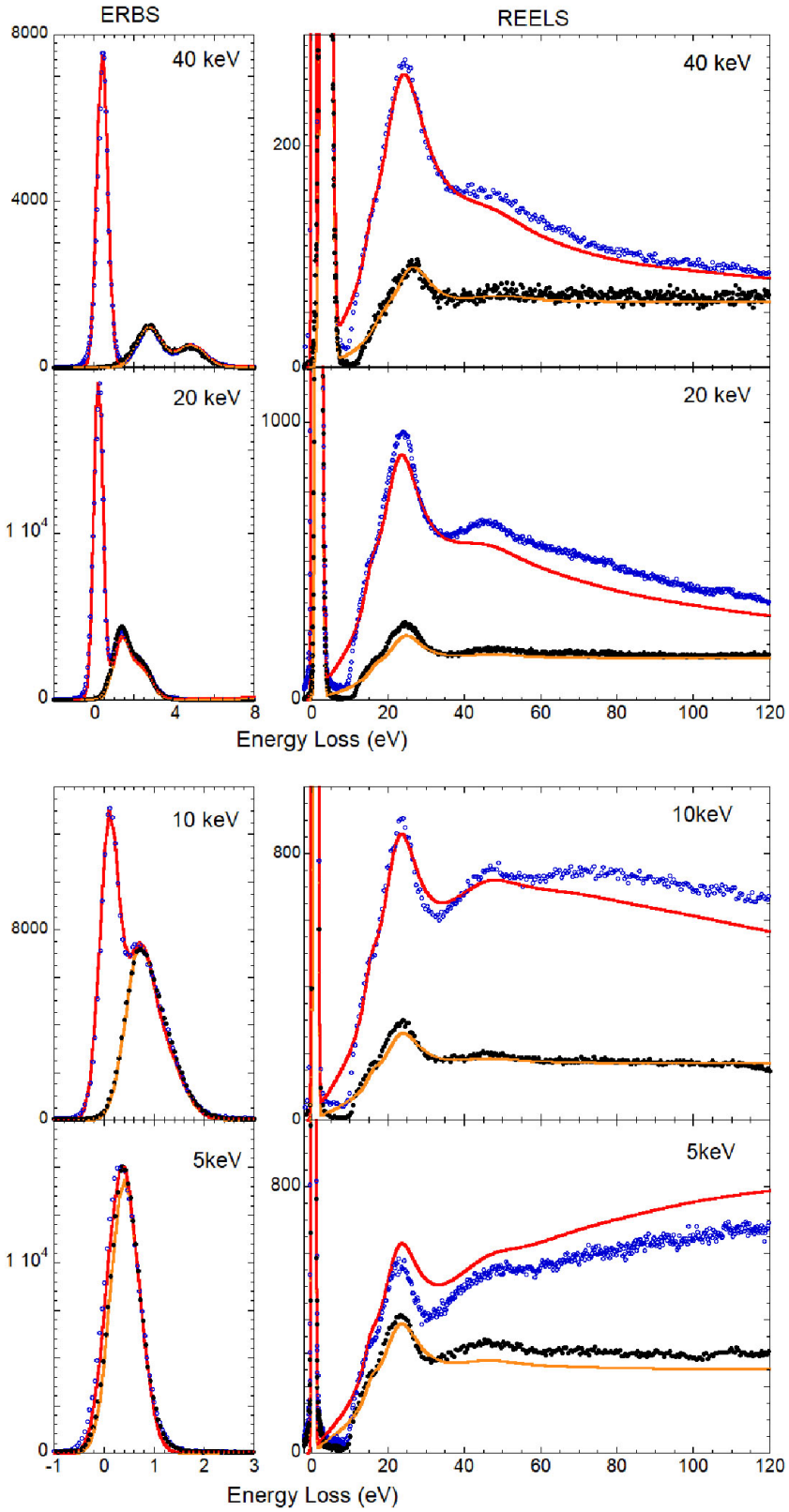

Figure 2. Measured spectra from 30 keV Au implanted SiO_2 samples using E_0 values between 5 and 40 keV (blue), compared to those of part of the sample that was not implanted (black). The Au contribution to the elastic peak decreases with decreasing E_0 values. The main differences in the energy loss part is at low ω values at high energies, but extends to large ω values for lower E_0 values. These trends are all reproduced by the calculation (lines).

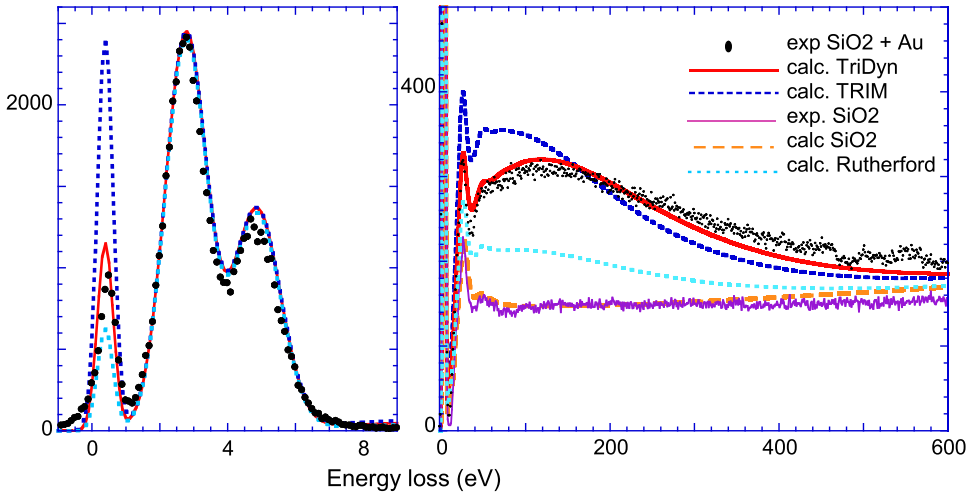

Figure 3. The measured spectra (dots) for 300 keV Au implanted SiO_2 compared to the calculated spectra based on the mean range and straggling of TRIM (dashed line) and TriDyn (full line). Only the TriDyn values describe the experiment well. The dotted line is based on a calculation using the Rutherford cross section (and TriDyn depth), rather than the ELSEPA one.

intensities were considered and the SiO_2 layer was taken to be 10 000 Å thick. Then, for $\omega < 600$ eV, the spectrum did not change any more if either N or the thickness (i.e. the depth up to which equation (5) is integrated) was increased.

With the same modification of the partial intensity of the implanted sample, we get the results shown also in figure 2. The elastic peak is well described and all the main changes in the REELS part of the spectrum were reproduced as well. Clearly the changes in the REELS spectrum are dominated by the enhanced backscattering probability due to Au with its very large DCS.

For the 300 keV implanted sample (fluence of 1×10^{16} cm^{-2}) the Au peak was less intense and the enhancement of the energy loss part extended to larger ω values, as is evident from figure 3. This all indicates that the Au is deeper in the sample as expected. For this case we calculated the expected spectrum based both on the depth distribution from TRIM-2013 and TriDyn (version 2017). Clearly the latter reproduces the experiment much better, both in the ERBS and REELS part of the spectrum. Thus, by combining the ERBS and REELS part of the spectrum the measurement is sensitive to both the amount of impurity present and its depth distribution. Ion based RBS also showed results consistent with the TriDyn predicted mean depth. The fact that in this case most of the implanted Au is beyond the SiO_2/Si interface and hence a small fraction of the electron trajectory is in Si, rather than SiO_2 is not taken into account in the simple model described here, but is not expected to change the result much. Indeed in the spectra of the sample without implantation we do not observe any noticeable features at energies where the Si layer start contributing as much as the SiO_2 layer. At these large energy losses, corresponding to larger depth, details of the shape of the loss function are not resolved anymore. Changes would be observed, of course, if the SiO_2 layer was grown on a high Z substrate, but in this case the average Z of the substrate and overlayer are not too different.

It is instructive to try to simulate the spectra based on the Rutherford cross section (DCS proportional to Z^2) rather than the ELSEPA one. Then the additional intensity due to Au is too low as is evident in figure 3. Changing the depth of the Au does not affect, within the v-shaped model, the additional intensity of the spectrum, just the energy loss at which it appears. There is thus no satisfactory description of the experiment possible based on the Rutherford cross section and the number of Au atoms present, as is known from the implanted fluence. These measurements are thus a confirmation of the validity of the ELSEPA cross sections under these conditions, where it is hard to test them otherwise. The physics behind the enhancement of the cross section relative to Rutherford (more than a factor of 2 for 40 keV electrons backscattered from Au) was described elsewhere [17].

5. Conclusion

In this paper we have shown that for the case of heavy impurities in relatively low-Z substrate the elastic peak and the energy loss part of a spectrum both contain information about the depth distribution of the heavy impurities. The experimental results can be reproduced using a simple model, based on partial intensity analysis and well-established elastic scattering cross sections. In the particular case of Au implanted SiO_2, studied here, it was only possible to fit the depth distribution using the TriDyn based range and straggling, and not using the TRIM/SRIM based one. We attribute this not to dynamical effects (e.g. sputtering), but to differences in the stopping used by both programs. In short we demonstrated a novel way of electron-beam based depth profiling. Depth resolution of the technique is about 20% of the electron inelastic mean free path.

Similar information, as obtained here, is also buried in the energy spectrum of electrons backscattered in a scanning electron microscope. More precise determination of their energy would enhance the 3D-compositional information obtained from such analysis greatly.

Acknowledgments

The authors want to thank Mr Hagege Abay Weldu for help with measurements, Felipe Ferreira Selau for the Au implantation, Bryan Tee for help with programming and Sanjoy Nandi for ellipsometry data.

ORCID iDs

M Vos https://orcid.org/0000-0003-2668-9216

References

[1] Went M and Vos M 2007 *Appl. Phys. Lett.* **90** 072104
[2] Werner W S M 2001 *Surf. Interface Anal.* **31** 141
[3] Cui Y-T, Tougaard S, Oji H, Son J-Y, Sakamoto Y, Matsumoto T, Yang A, Sakata O, Song H and Hirosawa I 2017 *J. Appl. Phys.* **121** 225307
[4] Zborowski C and Tougaard S 2019 *Surf. Interface Anal.* **51** 857
[5] Lloyd G E 1987 *Mineral. Mag.* **51** 3
[6] Ziegler J F 2004 *Nucl. Instrum. Methods Phys. Res.* B **219–220** 1027
[7] Ziegler J, Ziegler M and Biersack J 2010 *Nucl. Instrum. Methods Phys. Res.* B **268** 1818
[8] Möller W and Eckstein W 1984 *Nucl. Instrum. Methods Phys. Res.* **2** 814
[9] Jin K, Zhang Y, Zhu Z, Grove D A, Xue H, Xue J and Weber W J 2014 *J. Appl. Phys.* **115** 044903
[10] Vos M and Went M R 2006 *Phys. Rev.* B **74** 205407
[11] Forbes B D and Allen L J 2016 *Phys. Rev.* B **94** 014110
[12] Pines D 1963 *Elementary Excitations in Solids* (New York: Benjamin)
[13] Salvat F 2003 *Phys. Rev.* A **68** 012708
[14] Tahir D, Lee E K, Oh S K, Kang H J, Heo S, Chung J G, Lee J C and Tougaard S 2009 *J. Appl. Phys.* **106** 084108
[15] Shinotsuka H, Tanuma S, Powell C J and Penn D R 2015 *Surf. Interface Anal.* **47** 871
[16] Vos M, Grande P and Marmitt G 2018 *J. Electron Spectrosc. Relat. Phenom.* **229** 42
[17] Grande P L and Vos M 2013 *Phys. Rev.* A **88** 052901